SITE OCCUPANCY OF Co AND Ni IN ERYTHRITE–ANNABERGITE SOLID SOLUTIONS DEDUCED BY VIBRATIONAL SPECTROSCOPY

Wayde N. MARTENS[§], J. Theo KLOPROGGE, Ray L. FROST and Llew RINTOUL

Inorganic Materials Research Program, School of Physical and Chemical Sciences, Queensland University of Technology, GPO Box 2434, Brisbane, Queensland 4001, Australia

Abstract

Members of the solid-solution series between erythrite [$Co_3(AsO_4)_2 \cdot 8H_2O$] and annabergite [$Ni_3(AsO_4)_2 \cdot 8H_2O$] were synthesized and studied by a combination of X-ray diffraction, scanning electron microscopy, and Raman and infrared spectroscopy. The solid solution is complete, with the space group *C2/m* (monoclinic) being retained throughout. The unit-cell parameters decrease in size along all crystallographic directions as the amount of Ni increases. The β angle in the unit cell also decreases from 105.05(1)° (erythrite) to 104.90(1)° (annabergite). Crystals of annabergite and samples with a high Ni content are elongate along the *a* axis, and contrast with crystals of erythrite and Co-rich samples, which are elongate along *c*. In the Raman and infrared spectra of the synthetic samples, the band positions shift in accordance with the increase in bond strength associated with the decrease in the unit-cell parameters. Trends in positions of the antisymmetric arsenate stretching vibrations in the Raman spectra are sensitive to the site occupancy of metal ions in the structure. Changes in the crystal morphology, unit-cell parameters and vibrational spectra have been rationalized in terms of the site occupancy of Co and Ni in the structure. Substitution of Ni is directed to metal site 1 (C_{2h} site symmetry), whereas Co is directed to metal site 2 (C_2 site symmetry). Raman spectroscopy has proved to be useful for the determination of site occupancy of metal ions in solid solutions of minerals.

Keywords: erythrite, annabergite, cobalt arsenate, nickel arsenate, solid solution, Raman spectroscopy, vivianite-group minerals, infrared spectroscopy.

Sommaire

Nous avons synthétisé les membres de la solution solide entre l'erythrite [$Co_3(AsO_4)_2 \cdot 8H_2O$] et l'annabergite [$Ni_3(AsO_4)_2 \cdot 8H_2O$], et nous les avons caractérisés par diffraction X, microscopie électronique à balayage, spectroscopie de Raman et spectroscopie infrarouge. La solution solide est complète, toutes les compositions répondant au groupe spatial *C2/m* (symétrie monoclinique). Les paramètres réticulaires diminuent dans les trois directions cristallographiques à mesure que la proportion en Ni augmente. De plus, l'angle β de la maille élémentaire diminue, de 105.05(1)° (erythrite) à 104.90(1)° (annabergite). Les cristaux d'annabergite et les échantillons riches en Ni sont allongés selon l'axe *a*, tandis que les cristaux d'erythrite et les échantillons riches en Co le sont selon *c*. La position des bandes des spectres Raman et infrarouges de ces préparations synthétiques varie selon l'augmentation de l'intensité des liaisons associée à la diminution des paramètres réticulaires. Les déplacements des bandes de Raman dues aux vibrations antisymétriques d'étirement du groupe arsenate sont sensibles à la répartition des ions métalliques dans la structure. Nous adressons ces changements en morphologie, en paramètres réticulaires, et en spectres vibrationnels des cristaux selon la proportion de l'occupant du site (Co,Ni) dans la structure. L'incorporation du Ni implique le site 1 (symétrie du site: C_{2h}), tandis que le Co préfère le site 2 (symétrie du site: C_2). Les spectres de Raman s'avèrent utiles pour déterminer l'occupation des sites métalliques des minéraux montrant une solution solide.

(Traduit par la Rédaction)

Mots-clés: erythrite, annabergite, arsenate de cobalt, arsenate de nickel, solution solide, spectroscopie de Raman, minéraux du groupe de la vivianite, spectroscopie infrarouge.

[§] *E-mail address*: w.martens@qut.edu.au

Introduction

The vivianite-group minerals have a general formula $M^{2+}_3(XO_4)_2$•$8H_2O$, where M^{2+} may be Co, Fe, Mg, Ni, and Zn, and X = As or P (Anthony *et al.* 2000). Single-crystal X-ray-diffraction data have been used to determine the crystal structure of vivianite-type minerals. Wildner *et al.* (1996) established that the unit cell contains two formula units in the C^3_{2h} ($C2/m$) space group. In the unit cell, there are two sites occupied by two independent metal atoms (with C_{2h} and C_2 site symmetry, respectively), one independent arsenate–phosphate site (with C_s site symmetry), and two independent H_2O sites (both with C_1 site symmetry). The two metal-ion sites are typified by $M(1)O_2(H_2O)_4$ octahedra (C_{2h} site symmetry) and $M(2)_2O_6(H_2O)_4$ double-octahedron groups (C_2 site symmetry), wherein M is the metal cation. Further linkage is achieved *via* the XO_4 tetrahedra (X = As or P) to form complex sheets in (010), which are interconnected only by hydrogen bonds. Many studies of the vivianite group of minerals have shown that complex solid-solutions exist, for example with Co, Fe, Mg, Ni and Zn substitutions (Al-Borno & Tomson 1994, Amthauer & Rossman 1984, Ermolaev *et al.* 1977, Giuseppetti & Tadini 1982, Jambor & Dutrizac 1995a). Solid solutions of mixed phosphate–arsenates also are known in the vivianite group, but the extent of such substitutions is usually only minor.

In this study, synthetic erythrite – annabergite solid-solutions are investigated using a combination of X-ray diffraction, scanning electron microscopy (coupled with energy-dispersion X-ray analysis), and infrared and Raman spectroscopy. We focus on the site occupancy of the Ni and Co across the solid-solution series. If the substitution is ordered, then the underlying mechanism for this ordering will be further investigated as a part of a future study of solid-solution formation in vivianite-group minerals.

Previous Work

Wildner *et al.* (1996) characterized two naturally occurring samples of mixed-metal vivianite-group minerals, of chemical compositions $Co_{2.01}Fe_{0.74}Ni_{0.25}$ $(AsO_4)_2$•$8H_2O$ for erythrite and $Ni_{2.48}Mg_{0.50}Fe_{0.02}$ $(AsO_4)_2$•$8H_2O$ for annabergite, by X-ray diffraction, Mössbauer spectroscopy and electron-microprobe analyses. They found that the distribution of Mg^{2+} in annabergite shows a strong preference for the $M(2)$ sites over the $M(1)$ sites. In their work, Mössbauer spectroscopy of erythrite revealed an analogous preference of Fe^{2+} for the $M(2)$ site. Further evidence for ordered Mg and Ni at the two sites was also demonstrated for Mg-bearing annabergite (Giuseppetti & Tadini 1982). Erythrite with composition $(Co_{0.54}Mg_{0.29}Ni_{0.15}Zn_{0.02})_3(AsO_4)_2$•$8H_2O$ gives an indication of the complexity of solid solutions available to the vivianite-group minerals (Beyer 1978). Vivianite from the Big Chief pegmatite mine in Pennington County, South Dakota, USA, has a composition $Fe_{2.75}Mn_{0.30}Ni_{0.01}Ca_{0.05}(PO_4)_{2.03}$•$8H_2O$, with minor AsO_4, Na, Zn and Cu (Ritz *et al.* 1974). Even metal ions that do not form vivianite structures thus may substitute in the structure of vivianite-group minerals in small amounts. The vivianite group of minerals is an excellent choice for the study of solid solutions.

Experimental

Synthetic erythrite and annabergite solid-solutions were prepared by the slow addition (3.5 mL min^{-1}) of 1 L of 5.0×10^{-3} M, $Na_2H(AsO_4)$•$7H_2O$ to 2 L of 3.5×10^{-3} M cobalt–nickel sulfate solution at 80°C using a peristaltic pump. Under these experimental conditions, the solution remained acidic, which resulted in the incomplete precipitation of the minerals. This was evident because the supernatant solution remained colored from the remaining metal ions in the solution. The hydrated cobalt–nickel arsenate that precipitated from the solution was filtered and air-dried at ambient temperatures for 12 h. The crystals were hydrothermally treated at 80°C for 40 days in deionized water to increase crystallinity. Samples were analyzed for phase purity by X-ray diffraction and for chemical composition by electron-microprobe analysis.

Scanning electron microscopy (SEM) photographs were obtained on an FEI QUANTA 200 environmental scanning electron microscope operating at high vacuum and 20 kV. The system was coupled to an energy-dispersion X-ray spectrometer (EDS) with a thin Be window. Samples were fixed to an Al stub with C tape, prior to C-coating. Counts were accumulated over a period of 100 s using metal oxides as standards.

X-ray-diffraction patterns were collected using a Philips X'pert wide-angle X-ray diffractometer, operating in step-scan mode, with Cu$K\alpha$ radiation (λ 1.54052 Å). Patterns were collected in the range 2.5 to 75°2θ with a step size of 0.02° at a rate of 1° min^{-1}. Powder samples were applied with a sieve to a glass slide coated with petroleum jelly to ensure random orientation of the sample.

Rietveld analysis was performed using Rietica for Windows version 1.7.7 (Hunter 1998). All unit-cell parameters were allowed to vary; we used the data for erythrite published by Wildner *et al.* (1996) as starting parameters. Pseudo-Voigt peaks were used for the fit, with Lebail fitting strategy (Le Bail *et al.* 1988). A table of unit-cell parameters determined in this investigation has been sent to the Depository of Unpublished Data, National Research Council, Ottawa, Ontario K1A 0S2, Canada.

For Raman spectroscopy, the samples were placed on a polished metal surface on the stage of an Olympus BHSM microscope equipped with 10× and 50× objective lenses. The microscope is integrated to a Renishaw 1000 system, which in addition comprises

a monochromator, a Rayleigh filter system and a CCD detector. The samples were subjected to a focused beam from a Spectra-Physics model 127 He–Ne laser, producing highly polarized light at 633 nm, and spectra were collected at a resolution of better than 4 cm⁻¹ and a precision of ±1 cm⁻¹ in the range between 100 and 4000 cm⁻¹. Repeated acquisitions using the highest magnification (50×) were accumulated to improve the signal-to-noise ratio in the spectra. Spectra were calibrated using the 520.5 cm⁻¹ line of a silicon wafer. The spectra and the relevant digital files are available from the Depository of Unpublished Data, National Research Council, Ottawa, Ontario K1A 0S2, Canada.

Infrared spectra were obtained using a Nicolet Nexus 870 FTIR spectrometer fitted with a Smart Endurance single-bounce diamond ATR accessory. Spectra were collected over the 4000 to 525 cm⁻¹ range by the co-addition of 64 scans with a resolution of 2 cm⁻¹ and a mirror velocity of 0.6329 cm s⁻¹.

The manipulation of spectra, such as for baseline correction, was performed using the GRAMS software package (Galactic Industries Corporation, NH, USA). Band-component analysis was undertaken using the Jandel PEAKFIT software package, which enables the type of fitting function to be selected and allows specific parameters to be fixed or varied accordingly. Band fitting was done using a Lorentzian–Gaussian cross-product function with the minimum number of component bands used for the fitting process. The Gaussian–Lorentzian ratio was maintained at values greater than 0.7, and fitting was undertaken until reproducible results were obtained with squared correlations of R^2 greater than 0.995.

The spectra acquired in this investigation are available from the Depository of Unpublished Data, National Research Council, Ottawa, Ontario K1A 0S2, Canada.

RESULTS

Scanning electron microscopy

Figure 1 shows the cobalt mole fraction determined from EDS analysis as a function of the mole fraction of Co added to the reaction mixture. Specifically, the mole fraction of Co incorporated in the crystal structure of the precipitate is more than the mole fraction of Co of the starting solution. The amount of Co incorporated in the structure as a function of added Co may be described by Equations [1–3]:

$$N_m = 1.4601\ N_a + 0.0055$$
$$[0 < N_a < 0.45,\ R^2 = 0.997] \tag{1}$$

$$N_m = 0.7237\ N_a + 0.346$$
$$[0.45 < N_a < 0.7,\ R^2 = 0.991] \tag{2}$$

$$N_m = 0.4312\ N_a + 0.5582$$
$$[0.7 < N_a < 1,\ R^2 = 0.991] \tag{3}$$

where N_a is the mole fraction of Co in the preparation mixture, and N_m is the mole fraction measured in the precipitated mineral by SEM–EDS analysis.

SEM images (Fig. 2) show the crystals of (a) annabergite, (b) ~50% mixture of Co and Ni (measured) and (c) erythrite, with the indexing of the faces on the crystals used in the study shown in Figure 2d. Annabergite typically forms platelets, whereas erythrite forms needles. As the amount of Co in the crystal structure is increased, an elongation of the crystals in the *c* crystallographic direction is observed. In all samples, the *b* crystallographic direction is smaller than all other crystal directions, indicating that growth of (010) is slow.
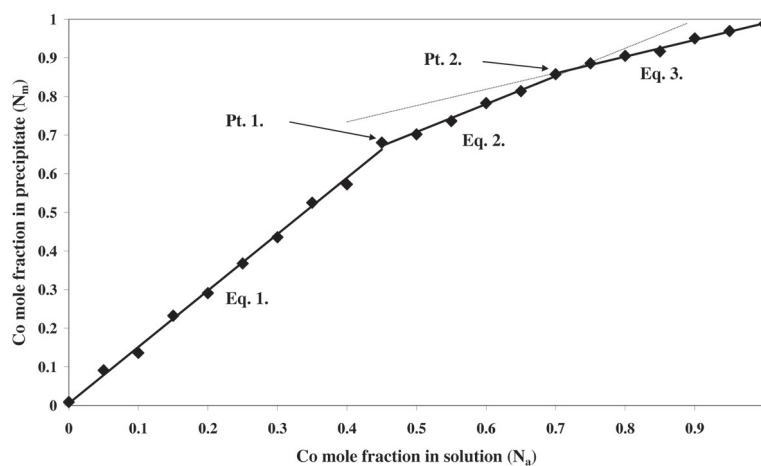

FIG. 1.   The concentration of Co in solution (N_a) *versus* Co measured by electron-microprobe analysis of the precipitates.

X-ray diffraction

X-ray-diffraction patterns of the solids are shown in Figure 3. Figure 4 shows the plots of the cell parameters obtained from the XRD patterns as a function of incorporated Co. The unit-cell parameters vary as a function of the amount of Co incorporated into the structure according to the following relations:

$$a = 0.0672 \ N_m + 10.158$$
$$[0 < N_m < 0.7, R^2 = 0.992] \tag{4}$$

$$a = 0.1402 \ N_m + 10.106$$
$$[0.7 < N_m < 1, R^2 = 0.96] \tag{5}$$

$$b = 0.1717 \ N_m + 13.287$$
$$[0 < N_m < 0.3, R^2 = 0.990] \tag{6}$$

$$b = 0.1138 \ N_m + 13.304$$
$$[0.3 < N_m < 1, R^2 = 0.98] \tag{7}$$

$$c = 0.044 \ N_m + 4.712 \ [R^2 = 0.993] \tag{8}$$

$$\beta = 0.1147 \ N_m + 104.87$$
$$[0 < N_m < 0.7, R^2 = 0.94] \tag{9}$$

$$\beta = 0.3686 \ N_m + 104.69$$
$$[0.7 < N_m < 1, R^2 = 0.96] \tag{10}$$

Vibrations of hydroxyl groups

The infrared spectra of the erythrite–annabergite solid solution in the hydroxyl-stretching region are shown in Figure 5. Previous studies have shown a
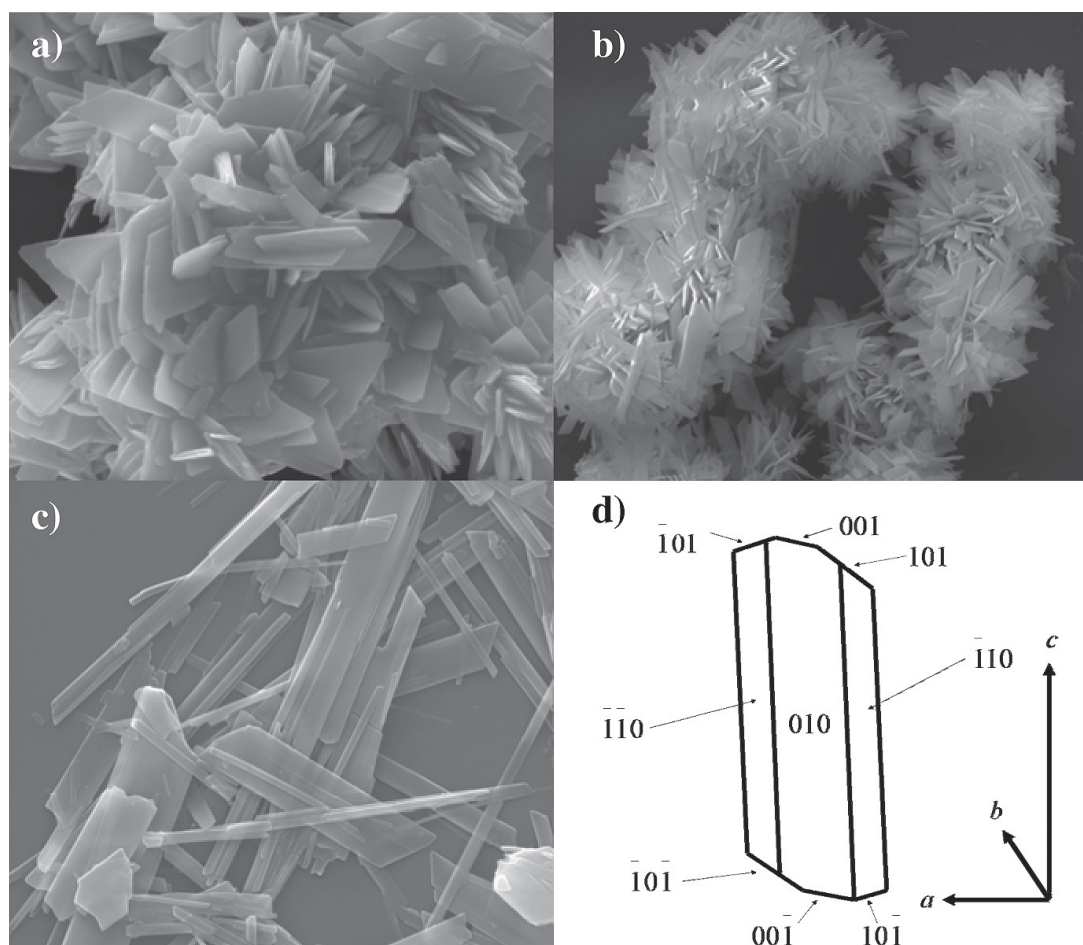

FIG. 2. (a) SEM image of annabergite (image width 10.89 μm); (b) SEM image of annabergite–erythrite solid solution (image width 43.39 μm) (mole fraction of Co 0.436); (c) SEM image of erythrite (image width 16.20 μm); (d) crystal indexing used.
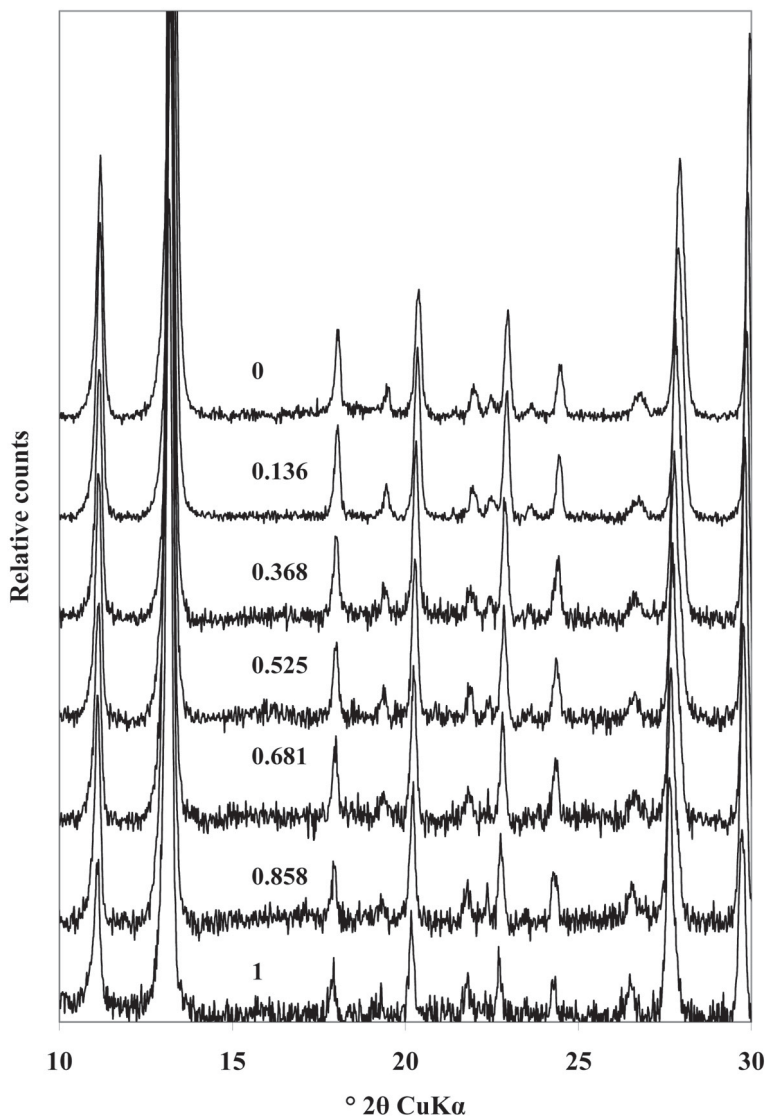
FIG. 3. X-ray-diffraction patterns of the erythrite–annabergite solid-solution series as a function of Co mole fraction.

strong correlation between OH-stretching frequencies and both the O...O bond distances and the H...O hydrogen-bond distances (Emsley 1980, Lutz 1995, Mikenda 1986, Novak 1974). Libowitzky (1999) showed that a regression function $\nu = 3592 - 304 \times 10^9 \exp(-d(O-O)/0.1321)$ cm^{-1}, wherein d is the bond distance in Å, exhibits regression coefficients better than 0.96. The erythrite–annabergite structure has two types of H_2O molecules. In erythrite, type-1 H_2O is

hydrogen-bonded at an average distance of 1.98(2) Å, whereas type-2 H_2O is hydrogen-bonded at an average distance of 2.04(2) Å (Wildner *et al.* 1996). Substituting these bond lengths into the above regression function indicates that the bands at ~3020 cm^{-1} are from type-1 H_2O and bands at ~3429 cm^{-1} are from type-2 H_2O (Martens *et al.* 2004). A plot of infrared band position *versus* mole fraction of Co shows a curved trend of the strongly and weakly hydrogen bonded H_2O molecule
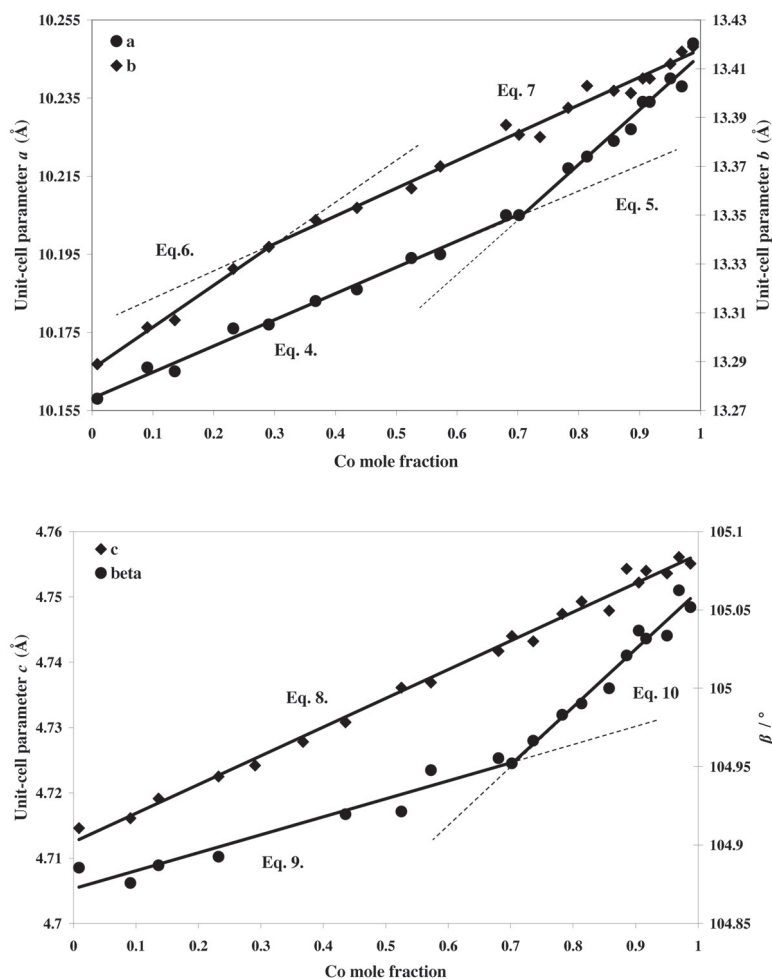
Fig. 4. Variation of unit-cell parameters as a function of mole fraction of Co. (a) a cell parameter and b cell parameter; (b) c parameter and β angle.

in the structure (Fig. 6). The trends show anomalies, in the form of high and low values, at Co mole fractions of ~0.33 and ~0.66.

Stretching vibrations in the arsenate tetrahedra

The infrared spectra of arsenate stretching and H_2O librational modes are depicted in Figure 7. This region is complex, with many overlapping librational modes of H_2O and arsenate modes. The modes at approximately 777 and 810 cm^{-1} are the arsenate v_3 modes, whereas the other modes in this region are due to librational modes of H_2O (Martens *et al.* 2004). The infrared-active v_1 arsenate mode is not evident (Martens *et al.* 2004). The Raman spectra show interesting trends of the arsenate stretching vibrations, as there is no change in the position of the symmetric stretching vibration, whereas the antisymmetric stretching modes shift in accordance with the degree of Co-for-Ni substitution. The A_g components of the v_3 Raman mode at 795 and 807 cm^{-1} (Martens *et al.* 2004) show a linear trend up to a Co mole fraction of approximately 0.66, after which the gradient of the trend changes distinctly (Fig. 8).

DISCUSSION

The X-ray-diffraction patterns and SEM photos (Figs. 2a–c, 3) confirm that the Ni–Co members form a solid-solution series. Crystals with high Ni contents are elongate along a, whereas samples with high Co
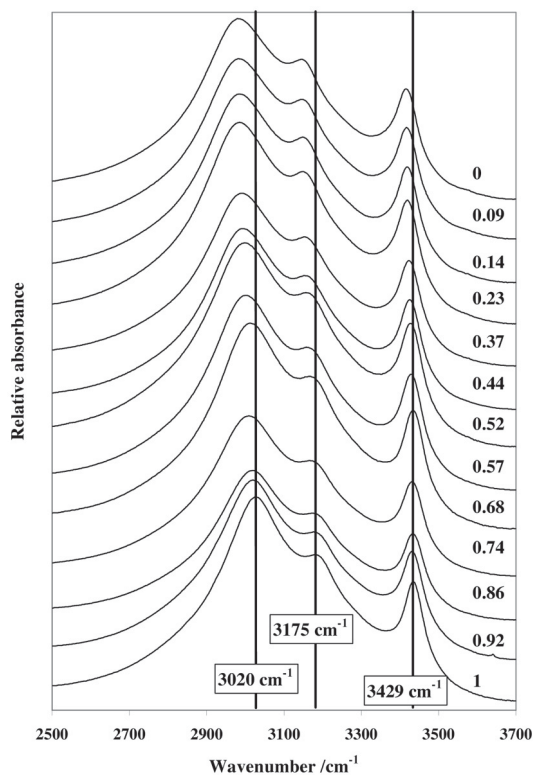
FIG. 5. Infrared spectra of the hydroxyl stretching region of $Co_xNi_{3-x}(AsO_4)_2 \cdot 8H_2O$ as a function of Co mole fraction.

contents are elongate along *c*. In all samples, growth in the *b*-axis direction is limited, primarily because of the hydrogen bonding in this direction, seen in the crystal as a perfect cleavage (Wildner *et al.* 1996). In solution, ions move in accordance to Brownian motion, with crystal growth only resulting from their collisions with the crystal faces. Crystal-growth kinetics are governed by: (1) the correct orientation of ionic groups in solution to be incorporated into the structure, and (2) the correct amount of energy to cause adherence of the ions to the surface of the crystal. The first factor is difficult to determine without knowledge of the speciation of the solution. The second effect is easy to consider in the case of (010), where only weak bonds exist (Wildner *et al.* 1996). On this crystal surface, only ions colliding with minimal amounts of kinetic energy will adhere, and so crystal growth along the *b* axis will lag behind that of the other crystallographic directions. In vivianite-group minerals, the (100) face has an equal number of alternating layers of site one and two, whereas the (001) face has a 5:6 ratio of *M*(1): *M*(2) (Wildner *et al.* 1996). The elongation in the *c* axis in the Co end-members may be explained if Co shows a preference to occupy *M*(2). Because *M*(2) is present in higher proportions on (001), growth along that plane is favored at high Co mole fractions. Conversely, at high Ni mole fractions, growth along (001) is suppressed, resulting in elongation along *a* for annabergite.

Figure 1 and Equations [1–3] show in broad terms that the relative proportion of Co to Ni in the solid solution was greater than the proportion present in the solution during synthesis. This effect may be related to the greater solubility of nickel arsenate ($K_{sp} = 1.9 \times 10^{-26}$) than cobalt arsenate ($K_{sp} = 7.6 \times 10^{-29}$) or may
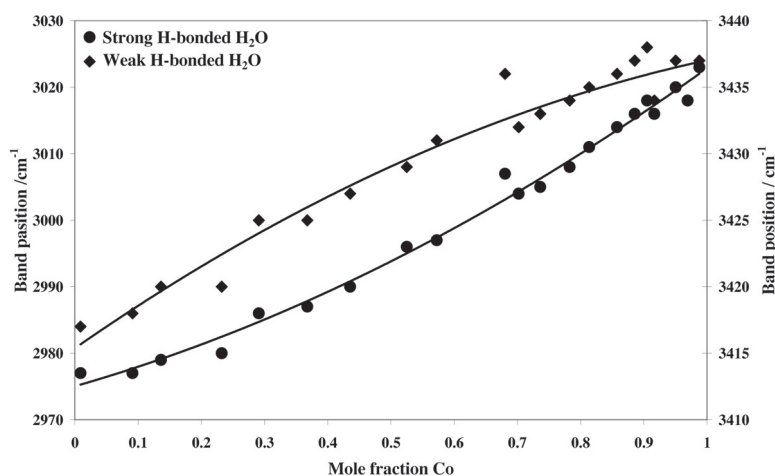

FIG. 6. Infrared band positions of weakly and strongly hydrogen-bonded H_2O as a function of incorporated Co.
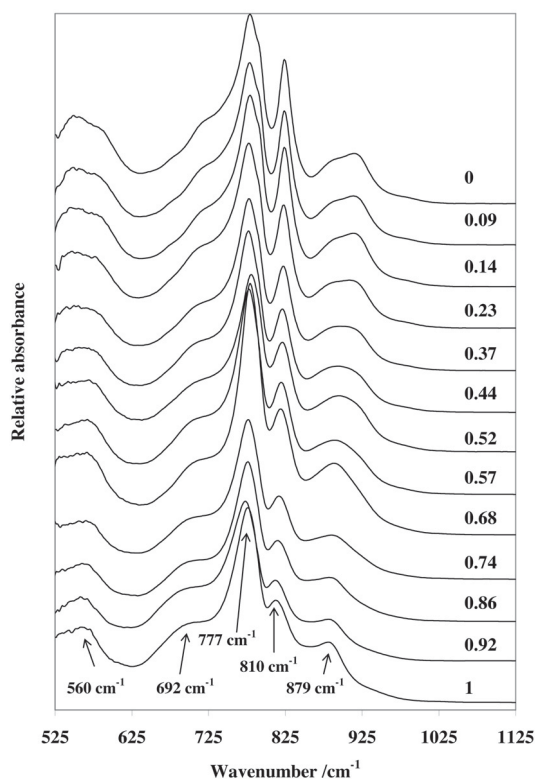
FIG. 7. Infrared spectra of the low-wavenumber region of $Co_xNi_{3-x}(AsO_4)_2 \cdot 8H_2O$ as a function of Co mole fraction.

be the manifestation of a partitioning, or site preference, of the metal ions. If, as previously suggested, Ni is preferentially incorporated at $M(1)$ and Co at $M(2)$, the uptake of Ni would lag that of Co because $M(2)$ has twice as many positions as $M(1)$. Similar effects have been observed by Jambor & Dutrizac (1995a, b) in the Ni–Mg series. It is, however, surprising to observe a similar effect in a Ni–Co series, when considering the similar size, electronegativity, and pattern of behavior of the two metal ions.

More specifically, Figure 1 shows a number of changes in the slope of the correlation between incorporated Co and added Co. These inflections provide strong evidence that Co is preferentially bound to $M(2)$. The first discontinuity in the linear trend takes place at a measured Co mole fraction of 0.66 (Fig. 1, pt. 1). This mole fraction corresponds to a metal site-ratio of two $M(2)$ sites to one $M(1)$. A second discontinuity occurs at an added Co mole fraction of 0.66 (Fig. 1, pt. 2). At this point, the preferred Co:Ni ratio of 2:1 is satisfied by the preparation mixture. The incorporation of Co is then further suppressed owing to the preference of Ni for $M(1)$, leading to a decrease in the slope to an added mole fraction of 1.

The size of the unit cell increases from annabergite to erythrite (Fig. 4, Eq. 4–10), owing to the larger ionic radius of Co, 0.75 Å, compared to that of Ni, 0.69 Å (Shanon & Prewitt 1969). The greater effective size of Co increases the relative spacing between the atoms in the ac plane, resulting in a larger β angle. However, it is also evident that for the unit-cell parameters a, b, and β, the increase occurs over two distinct linear segments. Parameters a and β increase with a relatively low slope from 0 to 0.66 Co mole fraction, and then with a higher
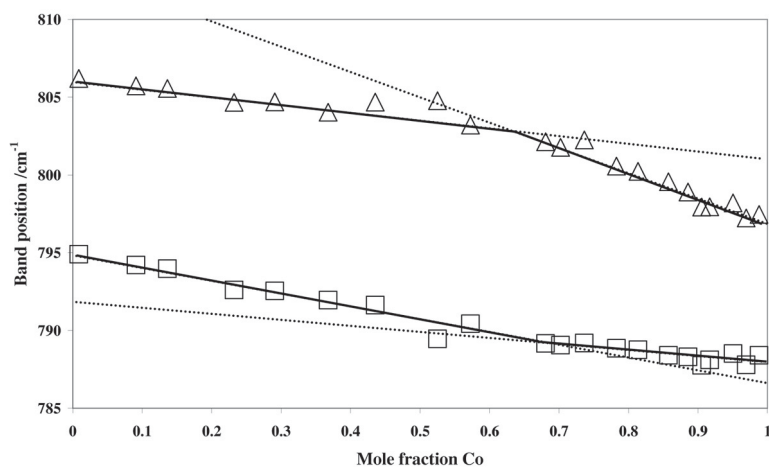

FIG. 8. Raman band positions of the A_g components of the ν_3 arsenate modes as a function of Co mole fraction.

slope from 0.66 to 1 Co mole fraction. At 0.66 Co mole fraction, $M(2)$ is fully occupied by Co, and further incorporation of Co can only occur through substitution at $M(1)$. It is the substitution and subsequent expansion of $M(1)$ that produce the higher slope above 0.66 Co mole fraction. In contrast, the b parameter shows a discontinuity at a Co mole fraction of 0.33, which is the point at which metal site 2 is exactly half filled with Co. From 0 to 0.33 mole fraction, Co is randomly incorporated at $M(2)$, but avoids those sites that already have one Co atom in the double octahedron; the effect is similar to that of the aluminum-avoidance rule for Al substitution for Si (Loewenstein 1954). Substitution continues until each double octahedron is occupied by one Ni atom and one Co atom. It is the incorporation of the initial Co at $M(2)$ and the subsequent increase in size of the site that cause the b parameter to rise rapidly at low Co mole fractions. Once half of all $M(2)$ sites have been occupied, further substitution of Co for Ni at $M(2)$ has a much reduced effect on size. Similar effects have been seen in the plagioclase series by other authors, Miyake et al. (2000) for example. The c parameter is affected equally by each metal site owing to the unit-cell structure in this direction, resulting in a linear expansion across the solid-solution range. The discontinuous nature of the trends in the plot of the unit-cell parameters as a function of the mole fraction of Co contrasts with the results of Jambor & Dutrizac (1995a, b), who obtained linear trends for all unit-cell parameters as a function of mole fraction of Co. The small deviations from linearity found in our study may not have been detected by Jambor & Dutrizac (1995a, b), because of their use of Debye–Scherrer films and fewer data points over the complete compositional range.

Infrared spectroscopic results show trends in the stretching region of the hydroxyl groups (Fig. 5) that are readily rationalized in terms of the site-preference scheme proposed above. There is a general increase in frequency of the hydroxyl-stretching vibrations from annabergite (Ni) to erythrite (Co) that is related to the overall increase in dimensions of the unit cell and the resulting decrease of interaction with near-neighbor atoms. Each of the two types of H_2O in the crystal structure of the mineral is located at an independent C_1 site. The H_2O at site 1 (W1) is bonded to $M(1)$, with strong H-bonding to neighboring atoms; H_2O at site 2 (W2), however, is bonded to $M(2)$, with weak H-bonding to neighboring atoms. Trends of the hydroxyl-stretching band of the strongly hydrogen-bound H_2O lag behind the addition of Co (Fig. 6). Because this H_2O is bonded to site 1, the position of this band is sensitive to changes in the site occupancy of $M(1)$. Thus the lag in the change in position of this band relative to the effect of the addition of Co indicates that $M(1)$ is preferentially occupied by Ni. In contrast, the trend in the stretching-band position of the weakly hydrogen-bonded H_2O (W2) anticipates that resulting from Co addition. Because W2 is bonded to $M(2)$, this effect indicates that Co is

preferentially incorporated at $M(2)$. If substitution were random, the variation of cell parameters and band positions would be expected to vary linearly, following the polarizing power of the metal (Chabanel et al. 1989, Dracopoulos et al. 1998, Kecki & Golaszewska 1967). These general trends are, however, convoluted owing to the effects of the Co-avoidance relationship and by the unit-cell effects as discussed above, thereby giving rise to the anomalies seen at the Co mole fractions of ~0.33 and ~0.66.

Plots of the position of the Raman band of the arsenate antisymmetric stretching frequencies (Fig. 8) as a function of Co mole fraction show a gradual linear trend up to a Co mole fraction of approximately 0.66, at which point the slope of the line changes toward a mole fraction of 1. Such a break is a clear indication that a crystallographic change has occurred (Comodi et al. 2001), and the occurrence of the discontinuity at 0.66 mole fraction means that the underlying cause is the difference in the occupancy of the metal-ion site. The difference in the slopes of the arsenate-stretching vibrations may be related to the relative polarizing power of the two metal ions. As the substitution of Co reaches a value that is greater than 0.66, $M(1)$ is occupied by Co, thereby decreasing the polarizing power on the oxygen atoms that would otherwise be coordinating the Ni cation. The slope of the lines up to the Co mole fraction of 0.66 shows the effect of the polarizing power of Ni at $M(2)$, whereas the slope of the line beyond a mole fraction of 0.66 shows the polarizing power of Co at $M(1)$. In the structure of annabergite, the arsenate ion has As–O bond lengths of 1.707(1), 1.686(1), and 1.686(1) Å for the oxygen atoms 1, 2 and 3 respectively, whereas in erythrite the analogous lengths are 1.714(2), 1.683(2), and 1.690(2) Å (Wildner et al. 1996). As a bond increases in strength, the vibrational frequency should also increase (Comodi et al. 2001), as is the case for the vibrational frequencies of the arsenate ν_3 modes in annabergite, which occur at a higher frequency than in erythrite. The ν_1 mode, however, does not increase from erythrite to annabergite, possibly because the decreased bond-distance of the metal to the oxygen of the arsenate in the annabergite series draws the electron density from the arsenic–oxygen bond, thereby offsetting the potential increased bond-strength arising from the contraction of the As–O bond. Further, the average As–O bond distance differs only marginally in the two minerals, with erythrite having an average distance of 1.694 Å and annabergite of 1.691 Å (Wildner et al. 1996). Considering this similarity and as the bond angles in the arsenate group are the same in the two minerals, it is not surprising that the symmetric stretching vibrations show little variation across the solid solution.

Figure 9 shows the splitting of the antisymmetric arsenate mode as a function of incorporated Co. In annabergite, $M(1)$ and $M(2)$ are occupied by Ni, making the oxygen atoms around the arsenate different only by
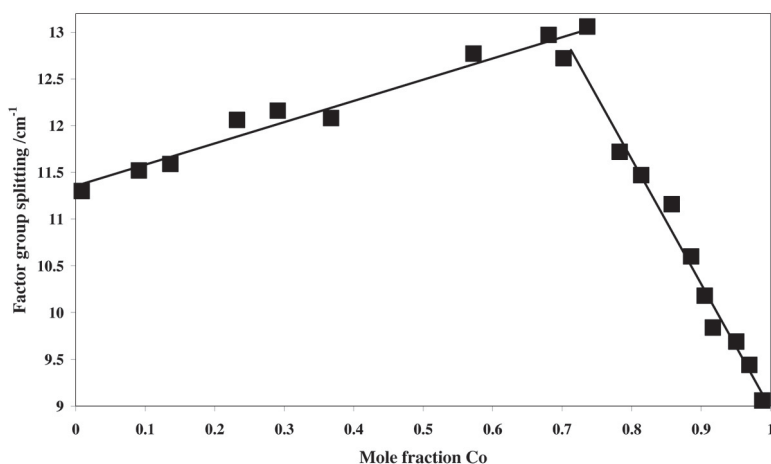
FIG. 9.   Raman arsenate ν_3 factor-group splitting as a function of Co mole fraction.

symmetry. Once the mole fraction of Co reaches 0.66, $M(2)$ is fully occupied by Co, and $M(1)$ is fully occupied by Ni. This partitioning amplifies the factor-group splitting, by increasing the differences of the oxygen atoms in the arsenate. At that point, not only do the sites differ by symmetry considerations, but also in electron density. This effect is at a maximum where $M(2)$ is fully occupied by Co and $M(1)$ is fully occupied by Ni. Beyond a Co mole fraction of 0.66, $M(1)$ becomes occupied by Co, which reduces this distortion, leading to a reduction in the splitting of the peaks (Fig. 9).

By close examination of peak positions, it is clear that with vibrational spectroscopy, one can detect changes in the structure of minerals. In particular, vibrational spectroscopy has proved to be a useful tool for the consideration of changes in the local environment of the arsenate ion and has provided strong evidence as to the site occupancy of metal ions in a solid solution.

Site selectivity

In the preparation of vivianite minerals, rapid rates of addition of solutions and the use of concentrated solutions lead to the formation of amorphous material rather than crystalline vivianite-type minerals (Jambor & Dutrizac 1995a, b). The slow crystallization of vivianite minerals thus seems dominated by thermodynamic considerations rather than kinetic factors, and even small variations in the selectivity of the metals at particular sites are likely to be manifested. Previous investigators have shown that in Mg-substituted annabergite, Mg shows a strong preference for $M(2)$ over $M(1)$ sites (Wildner *et al*. 1996, Rojo *et al*. 1996). Mössbauer spectroscopy of erythrite revealed an analogous preference of Fe^{2+} on the $M(2)$ site (Wildner *et al*. 1996). Rojo *et al*. (1996) considered this preference

in terms distortion of the two metal octahedra in the structure. Examination of the electronegativities of Ni (1.91), Co (1.88), Fe (1.83), Zn (1.65) and Mg (1.31) (Lide 2002) reveals, however, that in each case, the more electronegative metal prefers $M(1)$. This sequence suggests that in erythrite, Fe, Zn, and Mg would prefer $M(2)$, whereas Ni would prefer $M(1)$.

REFERENCES

AL-BORNO, A. & TOMSON, M.B. (1994): The temperature dependence of the solubility product constant of vivianite. *Geochim. Cosmochim. Acta* **58**, 5373-5378.

AMTHAUER, G. & ROSSMAN, G.R. (1984): Mixed valence of iron in minerals with cation clusters. *Phys. Chem. Minerals* **11**, 37-51.

ANTHONY, J.W., BIDEAUX, R.A., BLADH, K.W. & NICHOLS, M.C. (2000): *Handbook of Mineralogy: Arsenates, Phosphates, Vanadates*. Mineral Data Publishing, Tucson, Arizona.

BEYER, H. (1978): Minerals from the dumps of the stibnite veins of Ahrbrueck (Eifel), especially a find of cabrerite. *Aufschluss* **29**, 401-408.

CHABANEL, M., BENCHEIKH, A. & PUCHALSKA, D. (1989): Vibrational study of ionic association in aprotic solvents. 12. Isothiocyanate M(NCS) complexes of non-transition-metal ions. *J. Chem. Soc. Dalton* **11**, 2193-2197.

COMODI, P., LIU, Y. & FREZZOTTI, M.L. (2001): Structural and vibrational behaviour of fluorapatite with pressure. II. In situ micro-Raman spectroscopic investigation. *Phys. Chem. Minerals* **28**, 225-231.

DRACOPOULOS, V., GILBERT, B. & PAPATHEODOROU, G.N. (1998): Vibrational modes and structure of lanthanide fluoride–potassium fluoride binary melts LnF_3–KF (Ln = La, Ce, Nd, Sm, Dy, Yb). *J. Chem. Soc. Faraday* **94**, 2601-2604.

EMSLEY, J. (1980): Very strong hydrogen bonding. *Chem. Soc. Rev.* **9**, 91-124.

ERMOLAEV, M.I., BYKOV, M.M., KUDINOVA, L.M. & SKUF'IN, P.K. (1977): Preparation of water-soluble cobalt and nickel compounds from erythrin–annabergite minerals. *Zh. Prikl. Khim.* **50**, 1920-1922 (in Russ.).

GIUSEPPETTI, G. & TADINI, C. (1982): The crystal structure of cabrerite, $(Ni,Mg)_3(AsO_4)_2 \bullet 8H_2O$, a variety of annabergite. *Bull. Minéral.* **105**, 333-337.

HUNTER, B. (1998): Rietica – a visual Rietveld program. *International Union of Crystallography, Commission for Powder Diffraction, Newsletter* **20**.

JAMBOR, J.L. & DUTRIZAC, J.E. (1995a): Solid solutions in the annabergite – erythrite – hörnesite synthetic system. *Can. Mineral.* **33**, 1063-1071.

_____ & _____ (1995b): Solid solutions on the Co–Ni and Ni–Mg joins of the arsenate members of the vivianite group, and their environmental significance. *Process Mineral.* **13**, 239-248.

KECKI, Z. & GOLASZEWSKA, J. (1967): Interactions in solutions of polar substances as observed in the Raman effect. XI. Normal coordinate analysis of cation–acetonitrile complexes. *Rocz. Chem.* **41**, 1817-1823.

LE BAIL, A., DUROY, H. & FOURQUET, J.L. (1988): Ab-initio structure determination of $LiSbWO_6$ by X-ray powder diffraction. *Mat. Res. Bull.* **23**, 447-452.

LIBOWITZKY, E. (1999): Correlation of the O–H stretching frequencies and the O–H...H hydrogen bond lengths in minerals. *Monatsh. Chem.* **130**, 1047-1049.

LIDE, D.R. (2002): *CRC Handbook of Chemistry and Physics*. CRC Press, New York, N.Y.

LOEWENSTEIN, W. (1954): The distribution of aluminium in the tetrahedra of silicates and aluminates. *Am. Mineral.* **39**, 92-96.

LUTZ, H. (1995): Hydroxide ions in condensed materials – correlation of spectroscopic and structural data. *Structure and Bonding (Berlin)* **82**, 85-103.

MARTENS, W.N., KLOPROGGE, J.T., FROST, R.L. & RINTOUL, L. (2004): Single-crystal Raman study of erythrite, $Co_3(AsO_4)_2 \bullet 8H_2O$. *J. Raman Spectros.* **35**, 208-216.

MIKENDA, W. (1986): Stretching frequency versus bond distance correlation of O–D(H)...Y (Y = N, O, S, Se, Cl, Br, I) hydrogen bonds in solid hydrates. *J. Mol. Struct.* **147**, 1-15.

MIYAKE, A., KAWSUYUKI, K. & KITAMURA, M. (2000): Molecular dynamics simulation of Al/Si-ordered plagioclase feldspar. *Am. Mineral.* **85**, 1159-1163.

NOVAK, A. (1974): Hydrogen bonding in solids. Correlation of spectroscopic and crystallographic data. *Structure and Bonding (Berlin)* **18**, 177-216.

RITZ, C., ESSENE, E.J. & PEACOR, D.R. (1974): Metavivianite, $Fe_3(PO_4)_2 \bullet 8H_2O$, a new mineral. *Am. Mineral.* **59**, 896-899.

ROJO, J.M., MESA, J.L., PIZARRO, J.L., LEZAMA, L., ARRIORTUA, M.I. & ROJO, T. (1996): Spectroscopic and magnetic study of the $(Mg,M)_3(AsO_4)_2 \bullet 8H_2O$ ($M = Ni^{2+}, Co^{2+}$) arsenates. *Mat. Res. Bull.* **31**, 925-934.

SHANNON, R.D. & PREWITT, C.T. (1969): Revised values of effective ionic radii in oxides and fluorides. *Acta Crystallogr.* **B25**, 925-946.

WILDNER, M., GIESTER, G., LENGAUER, C.L. & McCAMMON, C.A. (1996): Structure and crystal chemistry of vivianite-type compounds: crystal structures of erythrite and annabergite with a Mössbauer study of erythrite. *Eur. J. Mineral.* **8**, 187-192.